scientific reports

Check for updates

OPEN

Structural and functional foetal renal abnormalities as a mechanism of oligohydramnios in a guinea pig model of growth restriction

Ayako Inatomi✉, Daisuke Katsura, Shinsuke Tokoro, Yuji Tanaka, Akiko Nakamura, Kaori Hayashi & Shunichiro Tsuji

In this study, we aimed to investigate the mechanisms underlying oligohydramnios in foetal growth restriction (FGR), focusing on the contribution of renal structural and functional abnormalities. A guinea pig model of maternal nutrient restriction (MNR) was established to induce FGR. Pregnant guinea pigs were divided into control and MNR groups. Foetuses were classified as appropriate for gestational age (AGA) or FGR based on body weight. Amniotic fluid and foetal kidneys were collected at gestational days 60–61. Amniotic fluid biomarkers were measured. Histopathology was performed to evaluate renal morphology. MNR resulted in a 25% reduction in foetal body and placental weights and a 50% reduction in amniotic fluid volume compared with AGA controls. Histological analyses revealed renal injury in FGR foetuses, characterised by podocyte foot process effacement, endothelial damage, and disruption of the tubular basement membrane. These structural abnormalities indicate impaired glomerular filtration and defective tubular reabsorption. Amniotic fluid concentrations of albumin, cystatin C, and liver-type fatty acid–binding protein were higher in FGR than in controls, reflecting glomerular leakage and tubular oxidative stress. These findings are consistent with reduced foetal urine production and development of oligohydramnios. They indicate that oligohydramnios in MNR-induced FGR is associated with compromised renal integrity.

Keywords Foetal growth restriction, Appropriate-for-gestational-age, Oligohydramnios, Renal abnormalities, Maternal nutrient restriction, Kidney

Abbreviations

FGR	Foetal growth restriction
MNR	Maternal nutrient restriction
AGA	Appropriate for gestational age
L-FABP	Liver-type fatty acid–binding protein
BUN	Blood urea nitrogen
ELISA	Enzyme-linked immunosorbent assay
TEM	Transmission electron microscopy
SEM	Scanning electron microscopy
SDS-PAGE	Sodium dodecyl sulphate–polyacrylamide gel electrophoresis
NAG	N-acetyl-beta-D-glucosaminidase

Foetal growth restriction (FGR) is a condition in which the foetus does not achieve the growth expected for its gestational age because of growth delay or arrest in utero[1,2]. FGR foetuses are prone to developing oligohydramnios because of uteroplacental dysfunction and blood flow redistribution, which diminishes renal perfusion, reducing foetal urine output and amniotic fluid volume[3–5]. Blood flow redistribution is a survival mechanism characterised by increased blood flow to vital organs such as the brain and decreased blood flow

Department of Obstetrics and Gynecology, Shiga University of Medical Science, Seta Tsukinowa-Cho, Otsu, Shiga 520-2192, Japan. ✉email: ayaina@belle.shiga-med.ac.jp

to non-essential organs such as the kidney. This mechanism occurs when the foetus is exposed to hypoxic conditions in utero[6]. The main source of amniotic fluid from approximately 20 weeks of gestation is foetal urine[7]. Reduced blood flow to the kidneys, the primary site of amniotic fluid production, leads to decreased urine output, resulting in reduced amniotic fluid volume. Therefore, the presence of oligohydramnios in FGR foetuses suggests a deterioration in foetal haemodynamics. FGR foetuses with oligohydramnios have a higher risk of adverse perinatal outcomes[8,9].

Clinically, severely growth-restricted foetuses may develop anhydramnios. Because amniotic fluid is primarily composed of foetal urine, significantly reduced urine output—without membrane rupture, infections, or renal malformations—suggests extreme foetal dehydration. However, because the placenta supplies water, severe dehydration causing anuria is unlikely. Although renal blood flow may decrease, it is usually insufficient to cause anuria. Moreover, Doppler ultrasonography in FGR foetuses can rarely detect absent renal blood flow[10]. Thus, reduced renal perfusion alone does not fully explain oligohydramnios, and its precise mechanisms remain unclear.

We, therefore, hypothesised that oligohydramnios in FGR foetuses may stem from organic kidney abnormalities. Using guinea pigs, which have a relatively long gestation among rodents, we established an FGR model to investigate its causes and underlying mechanisms. To evaluate renal involvement beyond haemodynamic redistribution, we selected three amniotic fluid biomarkers reflecting complementary aspects of renal integrity. Albumin was assessed as an indicator of increased glomerular permeability, cystatin C as a marker of impaired proximal tubular reabsorption, and liver-type fatty acid–binding protein (L-FABP) as a surrogate of proximal tubular oxidative stress and injury. Understanding this mechanism is essential not only for clarifying disease pathophysiology but also for developing diagnostic and therapeutic strategies in growth-restricted pregnancies.

Methods

Ethical approval

A guinea pig model of moderate maternal nutrient restriction (MNR) was used, following experimental protocols approved by the Animal Experimentation Committee of Shiga University of Medical Science (Approval No. 2023–3-9). All procedures complied with Japanese regulations, including the Act on Welfare and Management of Animals, the Standards for the Care and Management of Laboratory Animals and Relief of Pain, and the Fundamental Guidelines for Proper Conduct of Animal Experimentation and Related Activities in Academic Research Institutions under the Ministry of Health, Labour and Welfare, Japan. This study is reported in accordance with the ARRIVE guidelines.

Establishment of the animal model

Details regarding animal housing, maternal body weight, food intake, and pregnancy outcomes have been described previously[11]. Nulliparous female guinea pigs (Slc: Hartley, Japan SLC, Tokyo, Japan) were housed individually in a dedicated small animal facility with a 12-h light–dark cycle and a controlled temperature of 25 °C. Daily food intake and the oestrous cycle were monitored.

Female guinea pigs were randomly assigned to either the appropriate-for-gestational-age (AGA) Control group with ad libitum food intake (n = 12) or the MNR group (n = 13). The MNR group received 70% of the average daily food intake per kg of body weight starting 4 weeks before pregnancy. Females identified in oestrus were co-housed with males for 48–72 h, and vaginal plug detection confirmed successful mating. Thereafter, the females were moved to individual cages. Pregnancy was defined as the day prior to vaginal plug detection, designated as gestational day 0. The non-pregnant animals were re-mated during the next oestrous cycle.

For the first 34 days of pregnancy, the MNR animals were provided with 70% of the average food intake per kg of body weight compared with control animals. Starting on gestational day 35, the food intake of the MNR animals was increased to 90% of the average intake per kg of body weight in the control group. Throughout the experimental period, food intake was recorded daily and body weight was monitored weekly; food intake in the MNR animals was adjusted, as necessary.

Foetal growth status (AGA or FGR) was determined post hoc based on foetal body weight measured at necropsy, as detailed below.

Necropsy, tissue collection, and blood analysis

On gestational days 60–61 (term = 68 days), the female guinea pigs were weighed and administered subcutaneous injections of atropine (0.05 mg/kg; Nipro ES Pharma Co., Ltd., Tokyo, Japan) and buprenorphine (0.05 mg/kg; Nippon Shinyaku Co., Ltd., Kyoto, Japan). Anaesthesia was induced with isoflurane inhalation (3–5% for induction and 1–3% for maintenance; Viatris Pharmaceuticals, Canonsburg, PA, USA) and maintained during the procedure. A local injection of 3 mL 1% lidocaine (Shionogi Pharma Co., Ltd., Osaka, Japan) was administered to the abdominal skin, followed by midline laparotomy. Before delivery, each amniotic sac was punctured with a 25G needle, and the amniotic fluid was completely aspirated. The collected fluid was centrifuged and stored at -80 °C for subsequent analysis. Thereafter, the uterus was opened to deliver the foetuses, and the numbers of live and dead foetuses in each uterine horn were recorded. Gestational days 60–61 were selected because guinea pigs complete nephrogenesis during the foetal period, and at this stage of gestation immature nephron structures are rarely observed in our specimens.

Body and placental weights were measured for all live foetuses. Foetuses weighing ≥ 80 g in the AGA-Control group were classified as AGA-Control, whereas those weighing ˂80 g in the MNR group were classified as growth-restricted (FGR-MNR). These criteria were based on standards used in previous studies to categorise foetal weights in near-term guinea pigs[11,12]. This threshold is slightly higher than the strict 10th percentile of foetal body weight in our dataset derived from all offspring of AGA dams (approximately 78.2 g), but has been

empirically adopted in prior reports as a stable criterion for identifying near-term growth-restricted guinea pig foetuses. Based on this classification, a necropsy was performed on AGA foetuses from the control group and FGR foetuses from the MNR group.

For necropsy, sedation was achieved via intraperitoneal injection of medetomidine (0.3 mg/kg; Nippon Zenyaku Kogyo Co., Ltd., Fukushima, Japan), midazolam (4 mg/kg; Maruishi Pharmaceutical Co., Ltd., Osaka, Japan), and butorphanol (5 mg/kg; Meiji Animal Health Co., Ltd., Tokyo, Japan). A cardiac puncture was performed to collect 1–3 mL of blood into heparinised syringes, which were kept on ice; the foetuses were euthanised by exsanguination via cardiac puncture. Blood samples were centrifuged, and the plasma was aliquoted and stored at -80 °C until analysis. After thorough perfusion with phosphate-buffered saline, the brain, heart, liver, and kidneys were dissected and weighed. In addition, the gonads were extracted to determine foetal sex. Portions of the collected organs were fixed in 4% paraformaldehyde, and the other organs were snap-frozen in liquid nitrogen and stored at -80 °C for later analysis. The dams were euthanised following blood collection by inhalation of an overdose of isoflurane (5–6%; Viatris Pharmaceuticals, Canonsburg, PA, USA).

Biochemical analysis of blood and amniotic fluid

Blood urea nitrogen (BUN) and creatinine concentrations were measured using the Hitachi Automatic Analyzer 7170 (Hitachi, Ltd., Tokyo, Japan). The analyses were conducted by Oriental Yeast Co., Ltd (Tokyo, Japan).

Biochemical analyses of the amniotic fluid were performed using the enzyme-linked immunosorbent assay (ELISA), following the protocols provided by the manufacturers. Albumin concentrations were measured using the Guinea Pig Albumin ELISA Kit (No. CSB-E15765Gp; Wuhan Huamei Biotech, Wuhan, China), and cystatin C levels were determined using the Guinea Pig cystatin C ELISA Kit (No. MBS268891, Mybiosource, San Diego, CA, USA). The Guinea Pig Liver Fatty Acid Binding Protein ELISA Kit (No. MBS2600522, Mybiosource) was used for L-FABP analysis. Measurements were conducted using an Infinite® 200PRO microplate reader (TECAN, Männedorf, Switzerland). Amniotic fluid concentrations of albumin, cystatin C, and L-FABP were normalised to creatinine levels.

Histopathological examination

Tissue blocks for histochemical analysis were fixed in 4% paraformaldehyde for 24 h and immersed in 70% ethanol for 24 h. Thereafter, the tissues were embedded in paraffin, sectioned into 4-µm slices using a microtome, and mounted onto slides (Crest Coat Microscope Slides, Matsunami Glass Ind., Ltd., Osaka, Japan).

Prior to staining, all slides were deparaffinised in xylene at three 5-min intervals, followed by rehydration through a graded ethanol series (100, 100, 100, 90, and 70%) for 5 min each. Afterwards, the tissue sections were rinsed with deionised water for 5 min.

Haematoxylin and eosin (H&E) staining

Kidney sections were stained with H&E. Tissue sections were prepared as described above and immersed in Mayer's Haematoxylin Solution (Fujifilm Wako Pure Chemical Corporation, Osaka, Japan) for 5 min. The sections were subsequently rinsed under running water for 15 min. Afterward, the sections were stained with 1% Eosin Y Solution (Fujifilm Wako Pure Chemical Corporation, Osaka, Japan) for approximately 2 min, followed by dehydration through a graded ethanol series (70, 90, 100, and 100%). The sections were cleared in xylene at three 3-min intervals and mounted with PathoMount (Fujifilm Wako Pure Chemical Corporation, Osaka, Japan).

Immunohistochemical staining

Tissue sections were prepared as previously described. Antigen retrieval was performed by heating the sections in Tris–EDTA buffer (pH 9.0; 10 × G-Activate pH 9.0; GenoStaff Co., Ltd., Tokyo, Japan) in a microwave for 10 min. Blocking was performed using Blocking One Histo (Nacalai Tesque Inc., Kyoto, Japan) at 22 °C for 60 min. The sections were incubated overnight at 4 °C with the primary antibodies. The following primary antibodies were used: IL-6 (1:200; No. 21865–1-AP, Proteintech, Rosemont, IL, USA), IL-10 (1:200; No. 60269–1-IG, Proteintech, Rosemont, IL, USA), L-FABP (1:500; No. GTX109142, GeneTex, CA, USA), and CD10. CD10 was used as a proximal tubular marker and was detected with a mouse monoclonal antibody (1:50; No. ab951, Abcam, Cambridge, UK) in co-staining experiments with IL-6 and L-FABP, and with a rabbit polyclonal antibody (1:200; No. 18008–1-AP, Proteintech, Rosemont, IL, USA) in co-staining experiments with IL-10. Thereafter, the sections were incubated for 60 min with a secondary goat anti-rabbit CoraLite Plus 594 antibody (1:200, No. RGAR004, Proteintech, Rosemont, IL, USA) and goat anti-mouse CoraLite Plus 488 antibody (1:200, No. RGAM002, Proteintech, Rosemont, IL, USA). Subsequently, the slides were mounted using the Hard-Set Mounting Medium with DAPI (H-1500, Vector Laboratories, Inc., Newark, CA, USA). Images were captured using a Nikon AX with NSPARC (Nikon, Japan) confocal microscope.

Transmission electron microscopy (TEM)

The tissue samples were fixed in 2.5% glutaraldehyde (No. 073–0536, Fujifilm Wako Pure Chemical Corporation, Osaka, Japan) on ice for 2 h. After washing, the samples were fixed in 2.0% osmium tetroxide (No. 0018; TAAB Laboratories Equipment Ltd., Calleva Park Aldermaston, UK) on ice for 2 h. After washing, the samples were dehydrated using a graded ethanol series. The dehydrated samples were replaced with propylene oxide (No. 75–56-9, Nisshin EM Co., Ltd., Tottori, Japan) and embedded in resin. Polymerisation was performed in a 60 °C oven for 24 h.

Ultrathin sections were prepared and stained with 2% aqueous uranyl acetate for 2 h, followed by 5 min of staining with lead nitrate (No. 18–0875-2; Sigma-Aldrich, St Louis, MO, USA). The specimens were examined using a transmission electron microscope (HT-7800; Hitachi High-Tech Corporation, Japan).

Scanning electron microscopy (SEM)

The tissue samples were fixed in 2.5% glutaraldehyde (No. 073–0536, Fujifilm Wako Pure Chemical Corporation, Osaka, Japan) on ice for 2 h. After washing, the samples were fixed in 2.0% osmium tetroxide (No. 0018; TAAB Laboratories Equipment Ltd) on ice for 2 h. After washing, the samples were dehydrated using a graded ethanol series. The dehydrated samples were replaced with isoamyl acetate (No. 139–12,155, Fujifilm Wako Pure Chemical Corporation, Osaka, Japan) and dried for 1 h using a critical point dryer. A gold coating was applied to the samples, which were examined using a scanning electron microscope (JSM-7500FA, JEOL Ltd., Tokyo, Japan).

Western blotting

Preparation of kidney tissue homogenates

Frozen kidney tissues were cut into small pieces (10–20 mg) on ice and homogenised thoroughly using beads in a chilled radio-immunoprecipitation assay buffer (approximately 500 µL per 10 mg of tissue; No. R0246, Tokyo Chemical Industry Co., Ltd., Tokyo, Japan) containing protease (1:50, No. 25955, Nacalai Tesque, Inc.) and phosphatase inhibitors (1:100, No. 07575, Nacalai Tesque, Inc.). The homogenates were incubated on ice for 15 min, followed by centrifugation at 10,000 × g for 10 min at 4 °C. Supernatants were collected and used for further analysis. Total protein concentrations were measured using the Pierce™ BCA Protein Assay Kit (No. 23227, Thermo Fisher Scientific, Waltham, MA, USA) according to the manufacturer's protocol, and the samples were stored at -80 °C until further use.

Sodium dodecyl sulphate–polyacrylamide gel electrophoresis (SDS-PAGE) and western blot analysis

Protein samples were denatured and reduced by adding an equal volume of EzApply (No. AE-1430, Atto, Japan) and heated at 95 °C for 5 min. A total of 10 µg of protein per sample was separated using sodium dodecyl sulphate–polyacrylamide gel electrophoresis on Mini-PROTEAN® TGX™ 4–20% precast gels (No. 4561096, Bio-Rad Laboratories, Hercules, CA, USA) at 200 V for 35 min. Subsequently, the proteins were transferred to a 0.2-µm polyvinylidene difluoride membrane using the Trans-Blot® Turbo™ Transfer Pack (No. 1704156, Bio-Rad Laboratories) and the Trans-Blot® Turbo™ Transfer System (Bio-Rad Laboratories) at 25 V for 7 min.

Membranes were blocked with EzBlock Chemi (No. AE-1475, Atto, Japan) for 60 min, and they were incubated with the following primary antibodies at 23 ℃ for 60 min, depending on the target protein: horseradish peroxidase (HRP)-conjugated anti-β-actin (1:20,000, mouse, No. HRP-60008, Proteintech), IL-10 (1:2000, mouse, No. 60269–1-IG, Proteintech), IL-6 (1:2000, mouse, No. ab9324, Abcam), pSTAT3 (1:1000, rabbit, No. 9131, Cell Signaling Technology, Danvers, MA, USA), and STAT3 (1:2000, rabbit, No. 102532-AP, Proteintech).

Thereafter, the membranes were incubated with the following HRP-conjugated secondary antibodies for 60 min at room temperature: goat anti-mouse (No. RGAM001, Proteintech) and goat anti-rabbit (No. RGAR001, Proteintech). For antibody dilution, Can Get Signal solution 1 (No. NKB-101, Toyobo, Japan) was used for primary antibodies, and Can Get Signal solution 2 (No. NKB-101, Toyobo, Japan) was used for secondary antibodies and HRP-conjugated anti-β-actin.

Finally, chemiluminescence was generated using Chemi-Lumi One Super (No. 02230, Nacalai Tesque, Inc.), and images were captured using the FUSION imaging system (SOLO.7S.EDGE, Vilber Bio Imaging, Marne-la-Vallée, France). Protein bands were quantified using the ImageJ software version 1.54 (National Institutes of Health, Bethesda, MD, USA). Results were expressed as relative protein expression normalised to β-actin.

Statistical analysis

All statistical analyses were performed using SPSS version 26 (IBM Corp., Armonk, NY, USA). Maternal characteristics, including dam body weight and litter size, were compared between groups using the independent samples t-test.

To account for the hierarchical structure of the foetal data (multiple foetuses nested within each dam), we employed linear mixed-effects models with dam ID included as a random effect. Fixed effects included group (FGR vs AGA), sex (male vs female), and their interaction. Because no significant group × sex interactions were observed in any outcome, the results were presented from models excluding the interaction term for clarity. For amniotic fluid albumin, the random effect of dam variance was estimated as zero, indicating negligible between-dam variability; therefore, only residual variance was included in the final model. Estimated marginal means (LS-means) and their standard errors (SE) were obtained from the models. Pairwise comparisons between groups were adjusted using Bonferroni correction. Results are presented as LS-means ± SE, unless otherwise stated. Statistical significance was set at $P < 0.05$.

Results

Twelve guinea pig dams were assigned to the AGA-Control group and 13 to the FGR-MNR group. The mean body weight of the dams at the start of pregnancy was 670.8 ± 9.2 g in the AGA-Control group and 639.2 ± 10.1 g in the FGR-MNR group, without a significant difference ($P = 0.305$, t-test). At the time of caesarean section, the mean body weight of the dams was 1189.2 ± 19.0 g in the AGA-Control group and 960.4 ± 30.7 g in the FGR-MNR group, showing a significant difference ($P < 0.001$, t-test). The AGA-Control group delivered an average of 3.4 offspring per dam, whereas the FGR-MNR group delivered an average of 3.8 offspring per dam, with no significant difference in litter size ($P = 0.185$, t-test).

Using an 80-g threshold to classify foetal weight as AGA or FGR, the study included 33 foetuses (19 males and 14 females) in the AGA-Control group and 33 foetuses (14 males and 19 females) in the FGR-MNR group.

Foetal body weight was significantly higher in the AGA-Control group than in the FGR-MNR group (AGA: 84.902 ± 1.467 g vs FGR: 64.767 ± 1.448 g; $P < 0.001$; Table 1), representing a 24.8% reduction in FGR foetuses.

Parameter	AGA-Control Male	AGA-Control Female	FGR-MNR Male	FGR-MNR Female	Group effect (*P*)	Sex effect (*P*)	Dam variance (*P*)
Body weight (g)	86.694 ± 1.712	82.937 ± 1.873	65.344 ± 1.813	64.084 ± 1.709	**< 0.001**	0.0907	15.724 (*P* = 0.0501)
Brain (g)	2.760 ± 0.0300	2.679 ± 0.0327	2.539 ± 0.0316	2.451 ± 0.0299	**< 0.001**	**0.00106**	0.00512 (***P* = 0.0424**)
Placenta (g)	6.611 ± 0.261	6.129 ± 0.285	4.801 ± 0.276	4.625 ± 0.261	**< 0.001**	0.143	0.359 (*P* = 0.0518)
Liver (g)	4.477 ± 0.144	4.139 ± 0.160	3.342 ± 0.156	3.174 ± 0.144	**< 0.001**	0.0576	0.0898 (*P* = 0.105)
Left kidney (g)	0.501 ± 0.0260	0.460 ± 0.0280	0.352 ± 0.0270	0.365 ± 0.0267	**0.00935**	0.493	0.00468 (***P* = 0.0137**)
Right kidney (g)	0.478 ± 0.0261	0.455 ± 0.0278	0.347 ± 0.0267	0.353 ± 0.0266	**0.00176**	0.661	0.00528 (***P* = 0.00745**)
Amniotic fluid (mL)	4.400 ± 0.308	4.450 ± 0.290	2.215 ± 0.252	2.316 ± 0.231	**< 0.001**	0.711	0.266 (*P* = 0.0726)
Amniotic fluid (mL) / 100 g foetal body weight	5.040 ± 0.481	5.336 ± 0.449	3.349 ± 0.393	3.652 ± 0.355	**0.00181**	0.401	0.519 (*P* = 0.126)

Table 1. Quantitative Assessment of Foetal Growth Restriction Effects on Organ Development and Amniotic Fluid Volume. Data are presented as estimated marginal means ± standard error (SE) derived from linear mixed-effects models, including foetal group (AGA-Control vs FGR-MNR) and sex (male vs female) as fixed effects and dam ID as a random effect. 'Dam variance' represents the variance component attributed to the random effect of the dam. $P < 0.05$ is considered statistically significant. For body and organ weight analyses, the sample sizes were: AGA-Control Male (n = 19), AGA-Control Female (n = 14), FGR-MNR Male (n = 14), and FGR-MNR Female (n = 19). For amniotic fluid volume and amniotic fluid volume normalised to foetal body weight (mL/100 g), sample sizes were slightly smaller—AGA-Control Male (n = 8), AGA-Control Female (n = 10), FGR-MNR Male (n = 12), and FGR-MNR Female (n = 17)—because accurate volume measurement was not possible in some cases due to fluid loss during collection. AGA, appropriate-for-gestational-age; FGR-MNR, maternal nutrient restriction-induced foetal growth restriction.

Placental weight was also higher in the AGA-Control group (AGA: 6.381 ± 0.222 g vs FGR: 4.720 ± 0.219 g; $P < 0.001$; Table 1), a 25.8% reduction in FGR. Brain weight was 2.719 ± 0.0258 g in AGA-Control foetuses compared with 2.495 ± 0.0254 g in FGR-MNR foetuses ($P < 0.001$), an 8.7% decrease.

Left and right kidney weights were significantly higher in AGA-Control foetuses (left: 0.482 ± 0.0233 g vs 0.359 ± 0.0231 g, $P = 0.000935$; right: 0.467 ± 0.0237 g vs 0.350 ± 0.0234 g, $P = 0.00174$), corresponding to 28.0% and 27.1% reductions in FGR-MNR foetuses, respectively. Similarly, liver weight was greater in the AGA-Control group (AGA: 4.313 ± 0.121 g vs FGR: 3.261 ± 0.120 g; $P < 0.001$; Table 1), a 25.6% reduction. Amniotic fluid volume was 4.423 ± 0.241 mL in the AGA-Control group and 2.266 ± 0.195 mL in the FGR-MNR group ($P < 0.001$; Table 1). This difference remained significant after normalisation to foetal body weight (amniotic fluid volume per 100 g foetal body weight: 5.187 ± 0.364 vs 3.500 ± 0.294 mL/100 g in AGA-Control and FGR-MNR, respectively; $P = 0.00181$; Table 1).

Pathological evaluations of renal injury were conducted in AGA-Control and FGR-MNR foetuses. In FGR-MNR foetuses, H&E staining revealed typical features of tubular injury, including epithelial flattening, hydropic degeneration, vacuolisation, denucleation, and cast formation within the tubules (Fig. 1).

Furthermore, SEM images of the glomeruli showed marked reduction and loss of podocytes on the glomerular surface in the FGR-MNR group (Fig. 2). TEM analysis of the renal tubules confirmed disruption of the basement membrane (Fig. 3). These findings indicate that FGR causes organic damage to the renal tubular tissue. The FGR-MNR group exhibited foot process loss, endothelial cell injury, and disruption of the basement membrane compared to the AGA-Control group (Fig. 3).

Plasma analysis showed that BUN levels were significantly higher in FGR-MNR foetuses than in AGA-Control foetuses (AGA-Control: 19.603 ± 1.041 mg/dL vs FGR-MNR: 25.222 ± 1.005 mg/dL; $P = 0.000738$). In contrast, plasma creatinine levels did not differ significantly between the groups (AGA-Control: 0.889 ± 0.0360 mg/dL vs FGR-MNR: 0.959 ± 0.0353 mg/dL; $P = 0.177$).

In amniotic fluid, the albumin/creatinine ratio was markedly higher in FGR-MNR foetuses than in AGA-Control foetuses (AGA-Control: 183.006 ± 75.896 µg/mL vs FGR-MNR: 682.446 ± 75.896 µg/mL; $P < 0.001$; Table 2, Fig. 4A). Similarly, cystatin C/creatinine ratio (AGA-Control: 21.263 ± 4.053 ng/mL vs FGR-MNR: 41.166 ± 4.048 ng/mL; $P = 0.00186$; Table 2, Fig. 4B) and L-FABP/creatinine ratio (AGA-Control: 118.527 ± 26.033 pg/mL vs FGR-MNR: 223.875 ± 25.615 pg/mL; $P = 0.00803$; Table 2, Fig. 4C) concentrations were significantly elevated in the amniotic fluid of FGR-MNR compared with AGA-Control foetuses.

Western blot analysis showed that IL-6 protein expression, normalised to β-actin, was significantly higher in the FGR-MNR group than in AGA-Control group ($P < 0.001$) (Figs. 4D, E). In addition, phosphorylated STAT3 induced by IL-6 was detected in the FGR-MNR group (Fig. 4D). Moreover, IL-10 protein expression was significantly higher in the FGR-MNR group ($P < 0.05$) (Figs. 4D, F).

Immunofluorescence analysis demonstrated that IL-6, IL-10, and L-FABP were predominantly expressed in the proximal renal tubules of FGR-MNR foetuses (Figs. 5, 6, 7). IL-6 expression was markedly elevated in the proximal tubular epithelium of FGR-MNR foetuses, showing strong co-localisation with the proximal tubular marker CD10 (Fig. 5). In contrast, IL-10, an anti-inflammatory cytokine, was localised to the proximal tubules and exhibited increased expression in the FGR-MNR group compared with AGA-Controls (Fig. 6). Furthermore, L-FABP, a marker of tubular injury and stress, was mainly expressed in the proximal tubules and showed a pronounced increase in the FGR-MNR foetuses (Fig. 7).

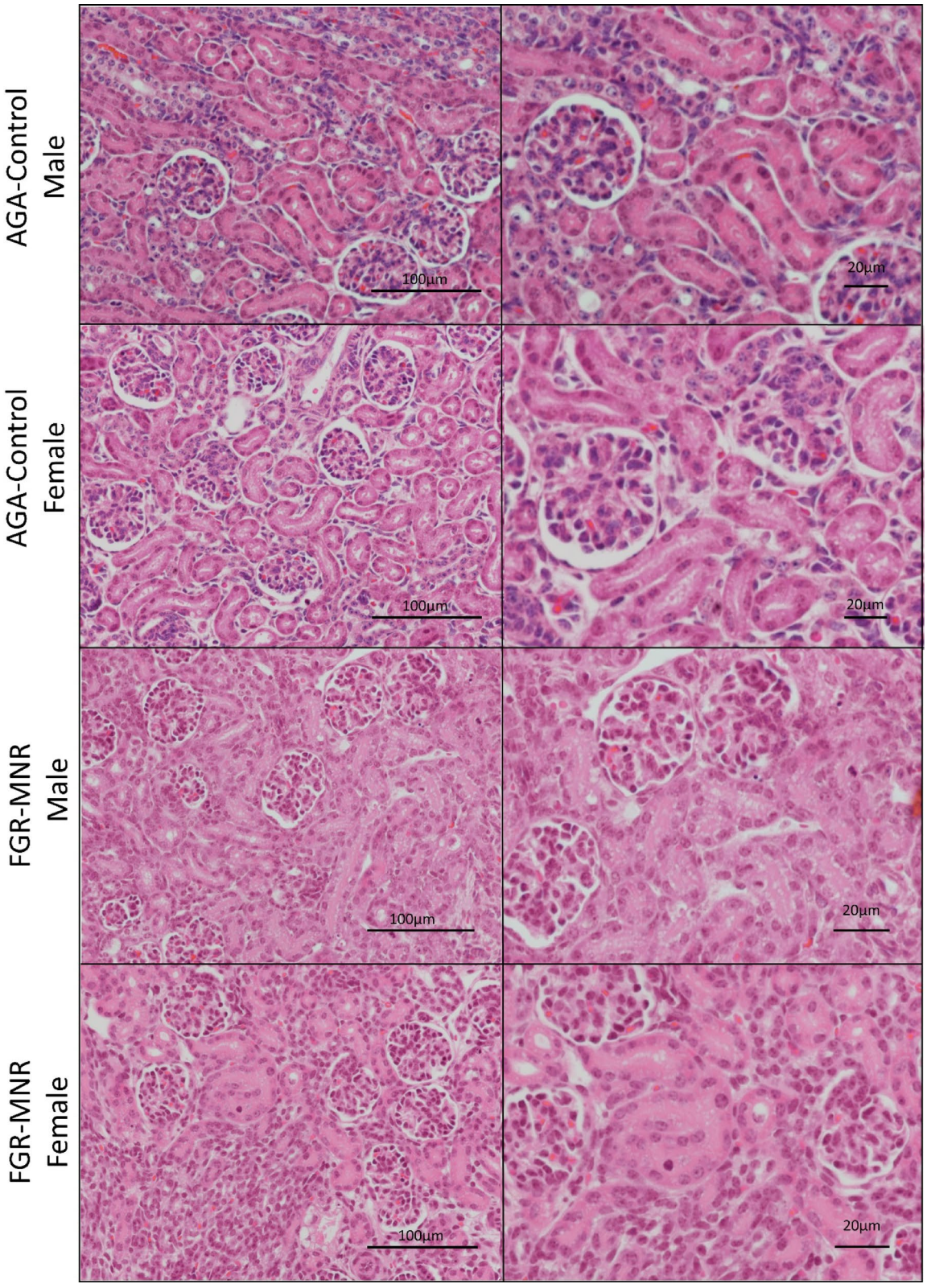


Fig. 1. Representative histological features of foetal kidneys in FGR-MNR and AGA-Control groups. Haematoxylin and eosin (H&E) staining of foetal kidneys from AGA-Control and FGR-MNR (maternal nutrient restriction-induced foetal growth restriction) foetuses. Both male and female foetuses are shown at low (left panels, scale bar = 100 µm) and high (right panels, scale bar = 20 µm) magnifications. Tubules in AGA-Control foetuses are structurally preserved, whereas kidneys of FGR-MNR foetuses exhibit characteristic features of tubular injury, including epithelial flattening, hydropic degeneration, cytoplasmic vacuolisation, denucleation, and tubular cast formation. AGA, appropriate-for-gestational-age; FGR-MNR, foetal growth restriction model: maternal nutrient restriction.

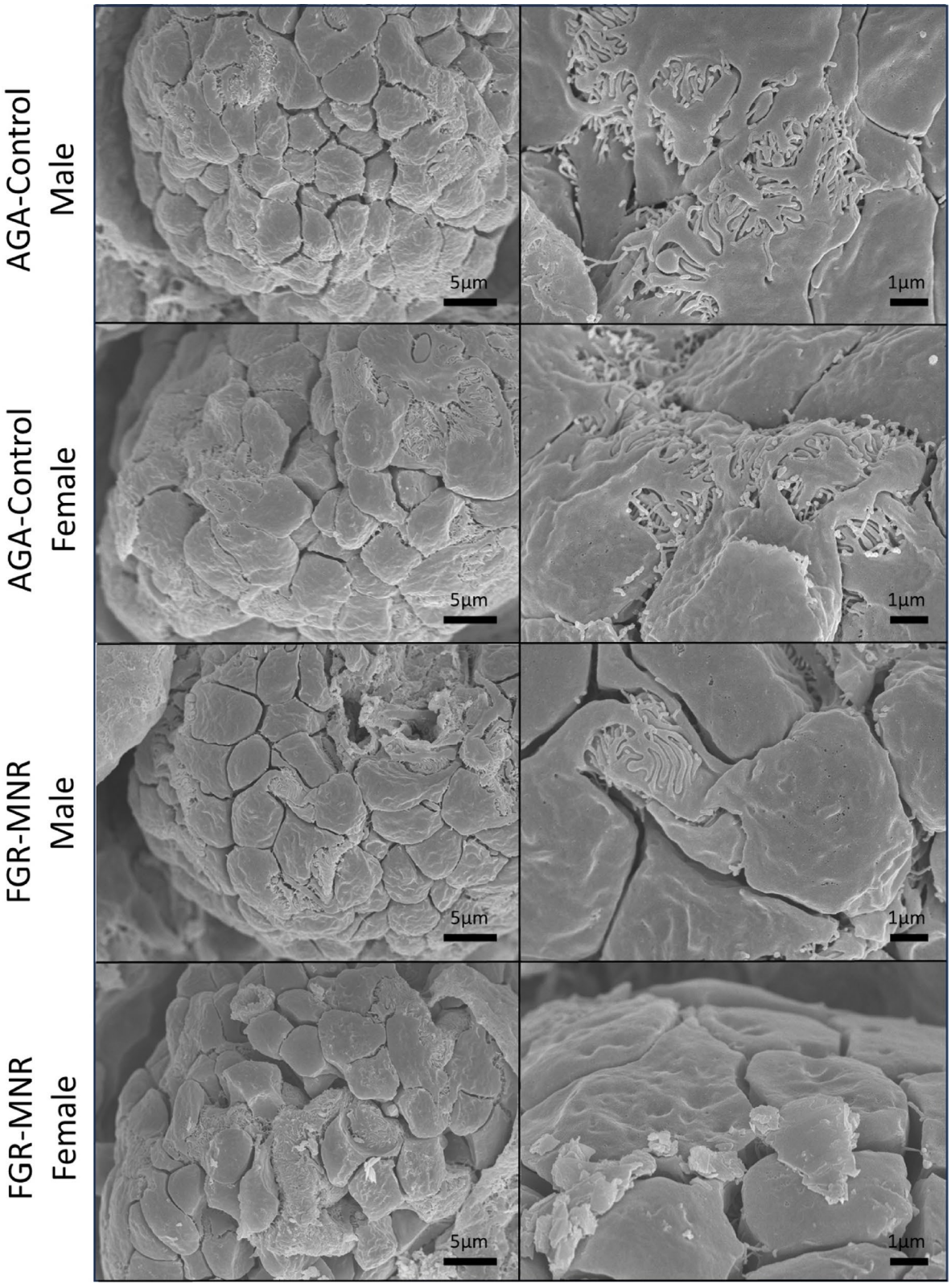


Fig. 2. Scanning electron microscopy (SEM) of glomerular ultrastructure in FGR-MNR and AGA-Control foetuses. Representative SEM images of glomeruli from AGA-Control and FGR-MNR (maternal nutrient restriction-induced foetal growth restriction) foetuses. Both male and female foetuses are shown at low (left panels, scale bar = 5 µm) and high (right panels, scale bar = 1 µm) magnifications. Analysis was performed on glomeruli located in the renal cortex. In AGA-Control foetuses, podocyte structures are well preserved, whereas in FGR-MNR foetuses the glomerular surface exhibits marked reduction and loss of podocyte coverage, with irregular flattening and partial detachment of podocyte foot processes. AGA, appropriate-for-gestational-age; FGR-MNR, foetal growth restriction model: maternal nutrient restriction.

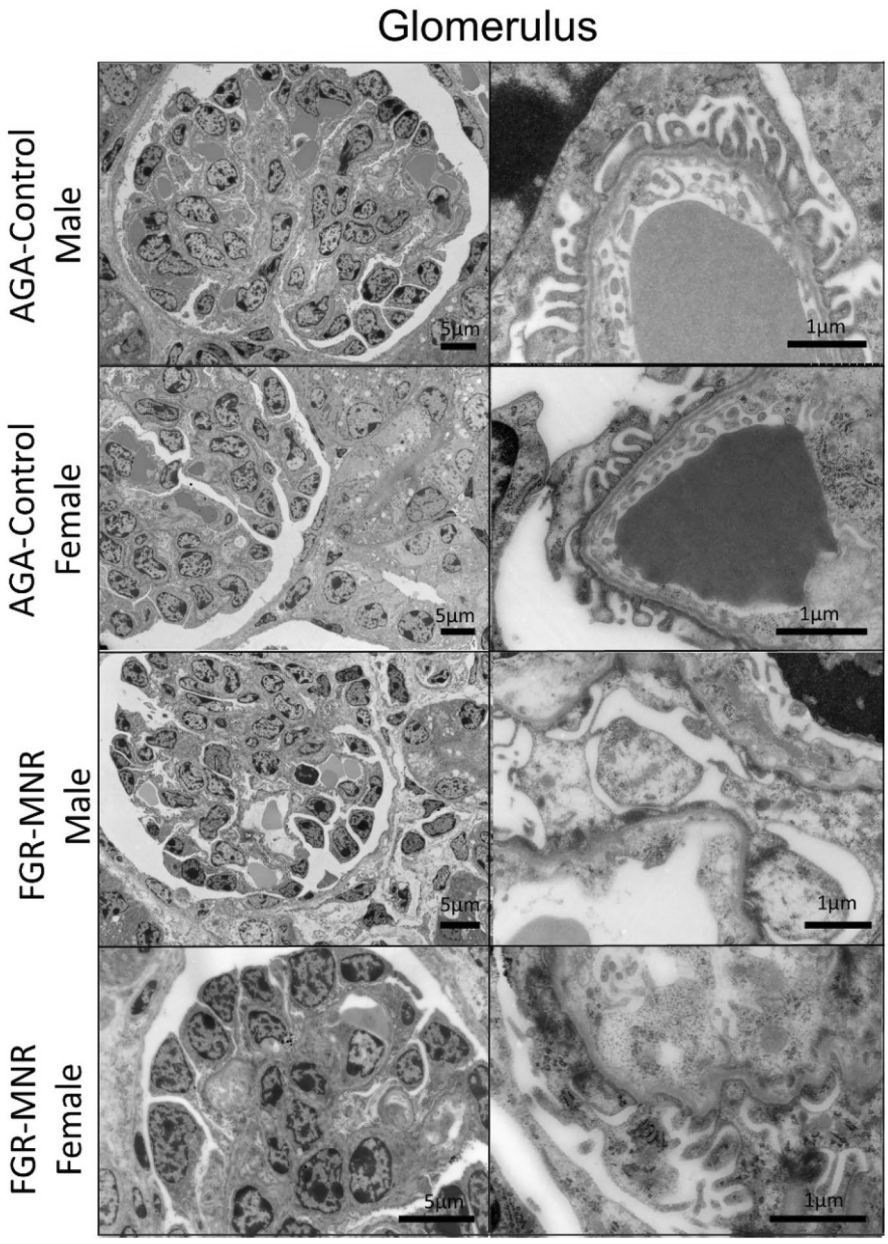


Fig. 3. Transmission electron microscopy (TEM) analysis of glomerular and tubular ultrastructure in FGR-MNR and AGA-Control foetuses. Representative TEM images of foetal kidneys from AGA-Control and FGR-MNR (maternal nutrient restriction-induced foetal growth restriction) foetuses. Both male and female foetuses are shown at low (scale bar = 5 µm) and high (scale bar = 1 µm) magnifications of glomerular and proximal and distal tubular ultrastructure. Analysis was performed on glomeruli located in the renal cortex. In AGA-Control foetuses, glomerular and tubular ultrastructure is intact, with well-preserved basement membranes. In contrast, FGR-MNR foetuses exhibit foot process effacement, endothelial cell injury, and disruption of the glomerular basement membrane. Proximal tubules show mitochondrial swelling and partial loss of the tubular basement membrane, indicating structural renal injury. AGA, appropriate-for-gestational-age; FGR-MNR, foetal growth restriction model: maternal nutrient restriction.

Discussion

Our FGR-MNR guinea pig model effectively replicated the asymmetric growth restriction and oligohydramnios that are characteristic of FGR. In addition, the average reduction in liver weight significantly exceeded that in the brain, consistent with previous findings[11,13]. This asymmetric growth restriction results from chronic changes in blood flow redistribution, prioritising vital organs, such as the brain, at the expense of other body tissues[14–16]. Beyond this well-known hemodynamic mechanism, our study newly demonstrates that intrinsic renal abnormalities are a direct cause of oligohydramnios in FGR. Specifically, histological and ultrastructural analyses revealed distinct glomerular and tubular structural abnormalities, indicating that impaired glomerular

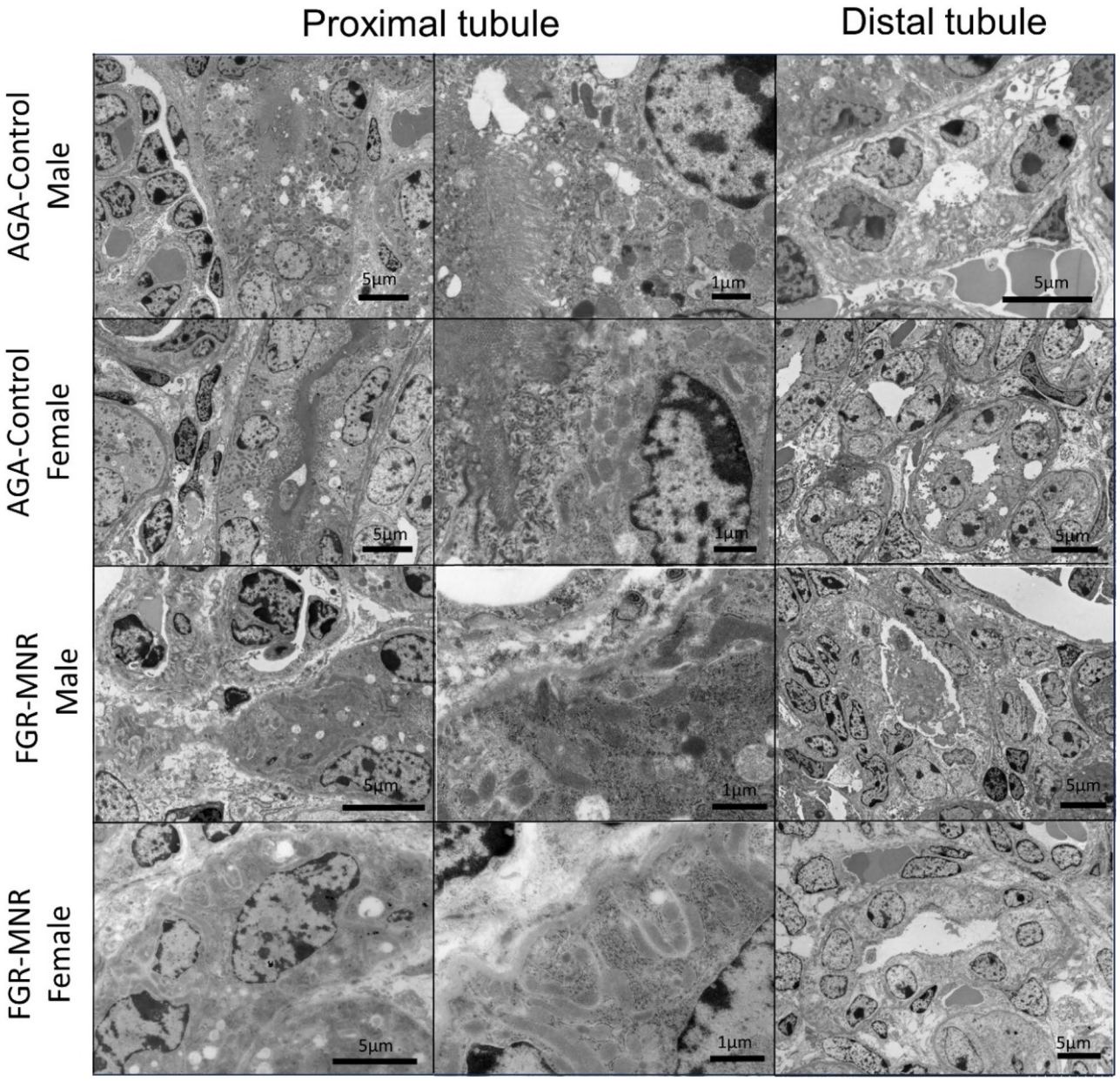


Fig. 3. (continued)

filtration and defective tubular reabsorption lead to decreased foetal urine production and, consequently, reduced amniotic fluid volume. Given the lack of definitive evidence regarding the causes of oligohydramnios, these findings represent a significant advancement in perinatal medicine.

Elevated levels of albumin, cystatin C, and L-FABP in the amniotic fluid provide evidence supporting organic renal abnormalities, which physiologically reflect reduced glomerular filtration and diminished tubular reabsorptive function. Damage to the glomerulus, a filtration apparatus for blood, injures the podocytes (glomerular components), leading to significant proteinuria[17,18]. In the present study, albumin levels in the amniotic fluid were significantly higher in the FGR-MNR group, corroborating the presence of glomerular injury.

Urinary cystatin C and L-FABP serve as indicators of tubular injury[19,20]. Monomeric cystatin C was found in the urine of neonates with FGR, which had significantly higher urinary cystatin C levels than appropriately grown neonates[21]. L-FABP is a next-generation biomarker for renal injury found in the cytoplasm of proximal tubular cells and expressed in the liver and proximal tubular epithelium[22–24], serving as a physiological marker of tubular oxidative stress and impaired reabsorptive function. Previously, we reported that elevated amniotic fluid L-FABP levels were related to FGR in human foetuses[25]. Furthermore, our studies demonstrated that amniotic fluid L-FABP levels were strongly correlated with foetal blood flow abnormalities, independent of other factors, and served as useful indicators of foetal hypoxia and overall foetal condition[26]. Taken together, these findings strongly suggest that amniotic fluid biomarkers function as physiological indicators of glomerular injury, tubular

Sample type	Parameter	AGA-Control Male	AGA-Control Female	FGR-MNR Male	FGR-MNR Female	Group effect (*P*)	Sex effect (*P*)	Dam variance (*P*)
Plasma	BUN (mg/dL)	19.600 ± 1.073	19.614 ± 1.083	25.320 ± 1.038	25.124 ± 1.038	**0.000738**	0.799	12.435 (***P*** **= 0.00117**)
	Creatinine (mg/dL)	0.880 ± 0.0408	0.899 ± 0.0423	0.965 ± 0.0405	0.954 ± 0.0400	0.177	0.919	0.0124 (***P*** **= 0.0135**)
Amniotic fluid	Albumin/Creatinine (μg/mL Cr)	154.297 ± 99.313	189.372 ± 112.610	474.997 ± 112.610	867.552 ± 99.313	**< 0.001**	0.0517	n.s
	Cystatin C/ Creatinine (ng/mL Cr)	19.618 ± 5.301	23.223 ± 5.954	42.142 ± 5.899	40.475 ± 5.301	**0.00186**	0.855	30.221 (*P* = 0.609)
	L-FABP/ Creatinine (pg/mL Cr)	99.435 ± 32.804	138.862 ± 37.536	212.399 ± 36.080	236.191 ± 32.794	**0.00803**	0.340	2120.325 (*P* = 0.382)

Table 2. Biochemical Evidence of Foetal Kidney Injury in Amniotic Fluid and Plasma. Data are presented as estimated marginal means ± standard error (SE) obtained from linear mixed-effects models, including foetal group (AGA-Control vs FGR-MNR) and sex (male vs female) as fixed effects and dam ID as a random effect. 'Dam variance' represents the variance component attributable to the random effect of the dam. BUN and creatinine were measured in foetal plasma (AGA-Control Male, n = 19; AGA-Control Female, n = 14; FGR-MNR Male, n = 14; FGR-MNR Female, n = 19), while albumin/creatinine, cystatin C/creatinine, and L-FABP/creatinine were measured in amniotic fluid (AGA-Control Male, n = 18; AGA-Control Female, n = 14; FGR-MNR Male, n = 14; FGR-MNR Female, n = 18). $P < 0.05$ is considered statistically significant. AGA, appropriate-for-gestational-age; FGR-MNR, maternal nutrient restriction-induced foetal growth restriction; L-FABP, liver-type fatty acid-binding protein; n.s., not significant.

oxidative stress, and reabsorption failure. The parallel elevations of albumin, cystatin C, and L-FABP in the amniotic fluid support the interpretation that structural renal injury has a direct physiological effect on foetal urine output and, thus, amniotic fluid balance.

Elevated amniotic fluid levels of N-acetyl-beta-D-glucosaminidase (NAG) have been reported in FGR cases[27]. NAG is highly concentrated in proximal tubular cells, and its levels increase in response to proximal tubular cell injury. Urinary neutrophil gelatinase-associated lipocalin levels in neonates with FGR were significantly higher than those in healthy neonates[28]. These findings support our study results and further confirm that oligohydramnios in FGR foetuses do not solely result from blood flow redistribution but are strongly associated with direct pathological conditions in foetal kidneys. Our findings, therefore, bridge morphological and biochemical evidence, linking renal structural damage to measurable physiological dysfunction.

Notably, the absence of significant sex effects suggests that renal vulnerability to nutrient restriction is not sexually dimorphic at this developmental stage. The inclusion of dam ID as a random effect confirmed that inter-dam variability contributed moderately to the overall variance but the primary determinant of renal impairment was foetal growth status. These findings indicate that oligohydramnios in FGR is closely related to intrinsic foetal renal injury rather than solely to placental insufficiency. This highlights the need to consider foetal kidney function as a key pathophysiological factor and a potential therapeutic target in growth-restricted pregnancies.

Structural abnormalities in the podocyte foot processes, which play a crucial role in maintaining the barrier function of podocytes, result from decreased ATP levels in podocytes during renal ischemia[29]. One proposed mechanism underlying glomerular damage-related tubular injury suggests that 'the reabsorption of large amounts of proteins leaked from the glomerulus by tubular cells results in tubular injury, which subsequently leads to renal dysfunction'[30,31]. Thus, our model supports a sequential mechanism: impaired placental perfusion and renal ischemia induce glomerular injury, excessive protein leakage, and subsequent proximal tubular overload and damage, culminating in reduced foetal urine output and oligohydramnios.

In the kidneys, pro-inflammatory cytokine IL-6 expression was elevated in FGR-MNR foetuses at the protein levels. Furthermore, phosphorylation of STAT3, a downstream signalling mediator of IL-6, was observed in the FGR-MNR group, supporting increased IL-6 expression. In acute kidney injury, increased IL-6 expression and STAT3 activation in renal tubular epithelial cells exert renoprotective effects[32]. In FGR, IL-6 may be induced by renal ischemia, and the induced IL-6 may contribute to renal protection.

Furthermore, the expression of IL-10 protein, an anti-inflammatory cytokine, was elevated. In the kidneys, dendritic cell-derived IL-10 provides significant endogenous protection against cisplatin-induced nephrotoxicity[33]. In the present study, immunohistochemical staining did not reveal IL-10 localisation in the renal interstitium. Moreover, previous studies have not identified IL-10 production in damaged proximal tubular epithelial cells. The mechanism underlying IL-10 production in damaged proximal tubular cells and its subsequent effects remain unexplored. In extremely preterm infants with FGR admitted to the neonatal intensive care unit, the umbilical cord blood levels of IL-6 and IL-10 were significantly higher in infants with brain injury than in those without brain injury[34]. These findings are consistent with the results of the present study.

FGR foetuses have an increased risk of end-stage renal disease[35–37]. The number of nephrons and filtration surface area are reduced in FGR kidneys[38–40], potentially contributing to future renal diseases. Reduced nephron number may contribute to decreased amniotic fluid volume during the foetal period. However, if nephron reduction alone was the cause of oligohydramnios, a persistent decrease in urine output would likely occur after birth. Thus, nephron reduction alone does not fully explain oligohydramnios, and its effect on amniotic fluid volume is limited. Our findings, therefore, suggest that transient but significant impairment of glomerular filtration and tubular reabsorption during foetal life plays a central physiological role in the reduction of amniotic fluid.

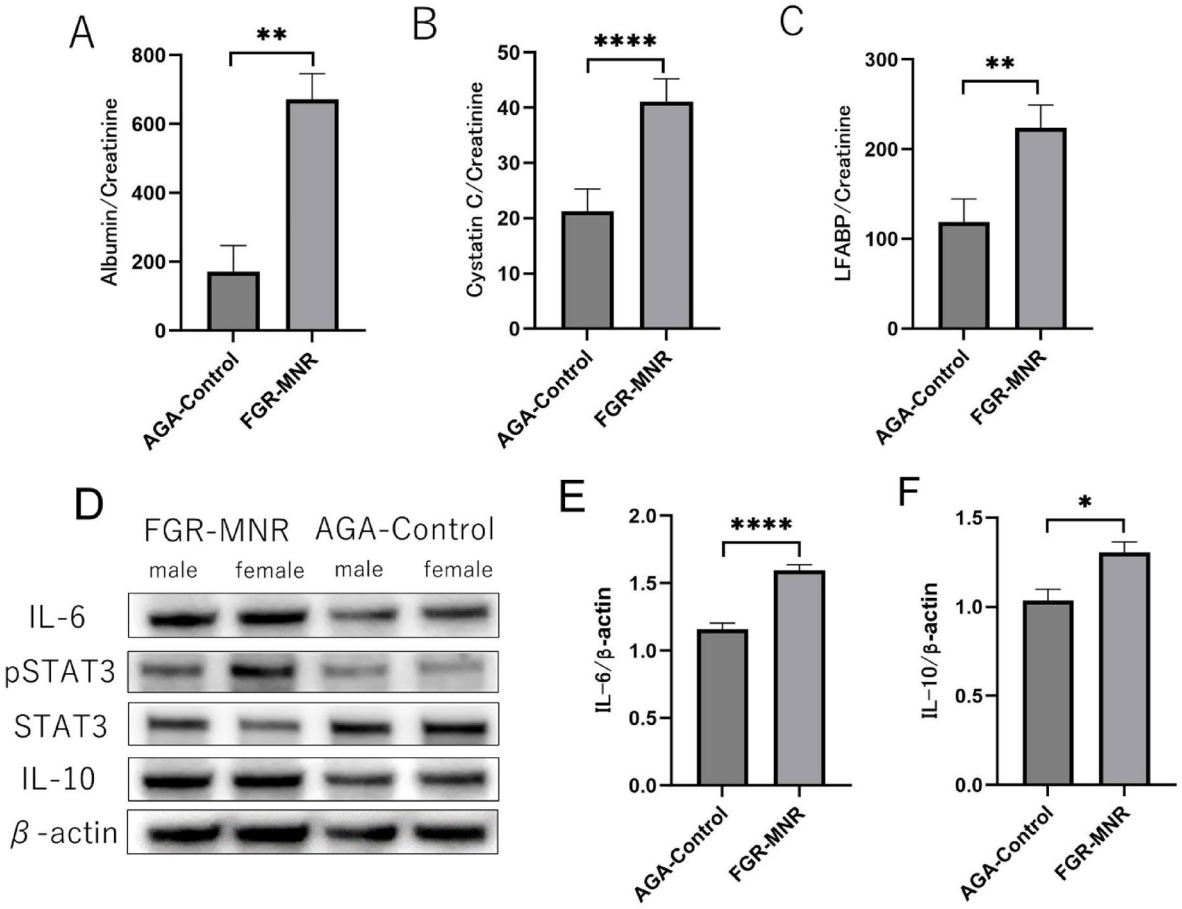


Fig. 4. Biochemical and inflammatory evidence of foetal renal injury in FGR-MNR foetuses. (A–C) Concentrations of amniotic fluid biomarkers, normalised to creatinine, in AGA-Control (n = 32) and FGR-MNR (maternal nutrient restriction-induced foetal growth restriction, n = 32) foetuses. (**A**) Albumin/creatinine (μg/mL), (**B**) cystatin C/creatinine (ng/mL), and (**C**) L-FABP/creatinine (pg/mL) are significantly elevated in the FGR-MNR group, indicating impaired renal function. (D) Representative Western blot images showing IL-6, phosphorylated STAT3 (pSTAT3), total STAT3, and IL-10 protein expression in foetal kidneys. β-actin was used as the loading control. Bands in Fig. 4 were cropped from the full-length blots shown in Supplementary Figure S1. Cropped areas are indicated by white boxes/lines. (**E**, **F**) Quantitative analyses of IL-6/β-actin and IL-10/β-actin ratios demonstrate significant upregulation of both inflammatory cytokines in the FGR-MNR group (n = 12) compared with the AGA-Control group (n = 12). Data are presented as estimated marginal means ± standard error (SE) derived from linear mixed-effects models including foetal group (AGA-Control vs FGR-MNR) and sex (male vs female) as fixed effects, and dam ID as a random effect. $^{*}P < 0.05$, $^{**}P < 0.01$, $^{***}P < 0.001$. AGA, appropriate-for-gestational-age; FGR-MNR, foetal growth restriction model: maternal nutrient restriction.

This study has some limitations. First, although the guinea pig model of MNR provides a physiologically relevant system for investigating human-like placental and renal development, species-specific differences limit the direct extrapolation of these findings to human pregnancies. Second, while structural and inflammatory alterations were identified, the precise molecular mechanisms underlying tubular and glomerular injury remain to be elucidated. Third, postnatal assessments—such as determining whether kidney damage sustained in utero can recover after birth—were not performed, limiting our understanding of the long-term implications of foetal renal injury.

This study suggests that oligohydramnios associated with FGR may arise not only from blood-flow redistribution and placental insufficiency but also from intrinsic renal alterations. Structural and functional changes—particularly those affecting glomerular filtration and tubular reabsorption—are consistent with reduced foetal urine production. Elevated amniotic fluid biomarkers such as albumin, cystatin C, and L-FABP may serve as physiological indicators of these renal alterations, integrating structural, biochemical, and functional evidence. Recognising foetal renal dysfunction as a potential contributor to oligohydramnios offers a translational framework for improving diagnostic approaches and exploring renal-protective strategies in growth-restricted pregnancies.

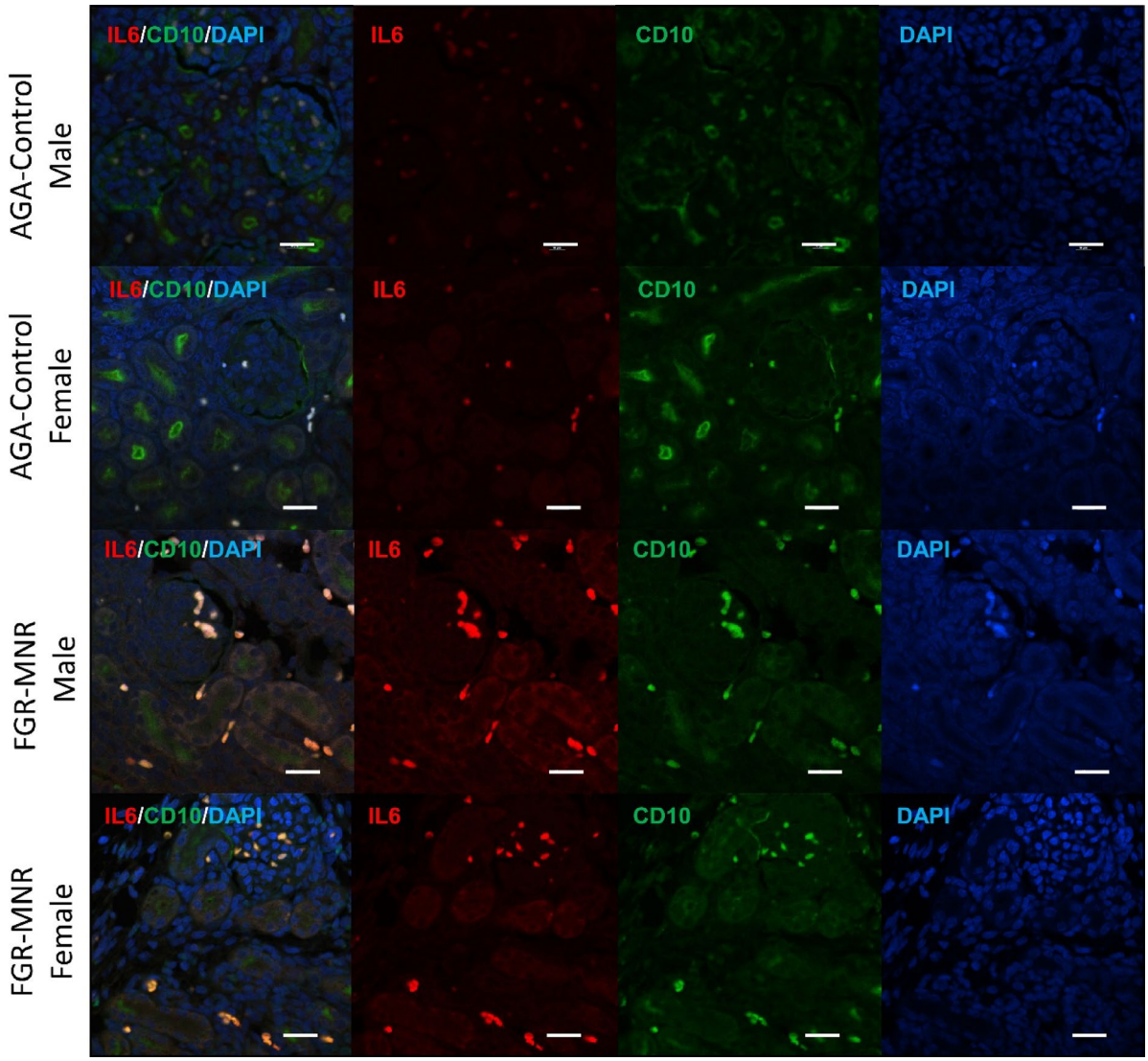


Fig. 5. Immunofluorescence localisation of IL-6 and CD10 in foetal kidneys from FGR-MNR and AGA-Control groups. Representative immunofluorescence images showing interleukin-6 (IL-6, red), CD10 (a proximal tubular marker, green), and nuclear counterstaining with DAPI (blue) in foetal kidneys from male and female guinea pigs of the AGA-Control and FGR-MNR groups. Merged images (IL-6/CD10/DAPI) demonstrate marked up-regulation of IL-6 expression in the renal tubules of FGR-MNR foetuses compared with AGA-Controls. Scale bars = 20 μm. AGA, appropriate-for-gestational-age; FGR-MNR, foetal growth restriction model: maternal nutrient restriction.

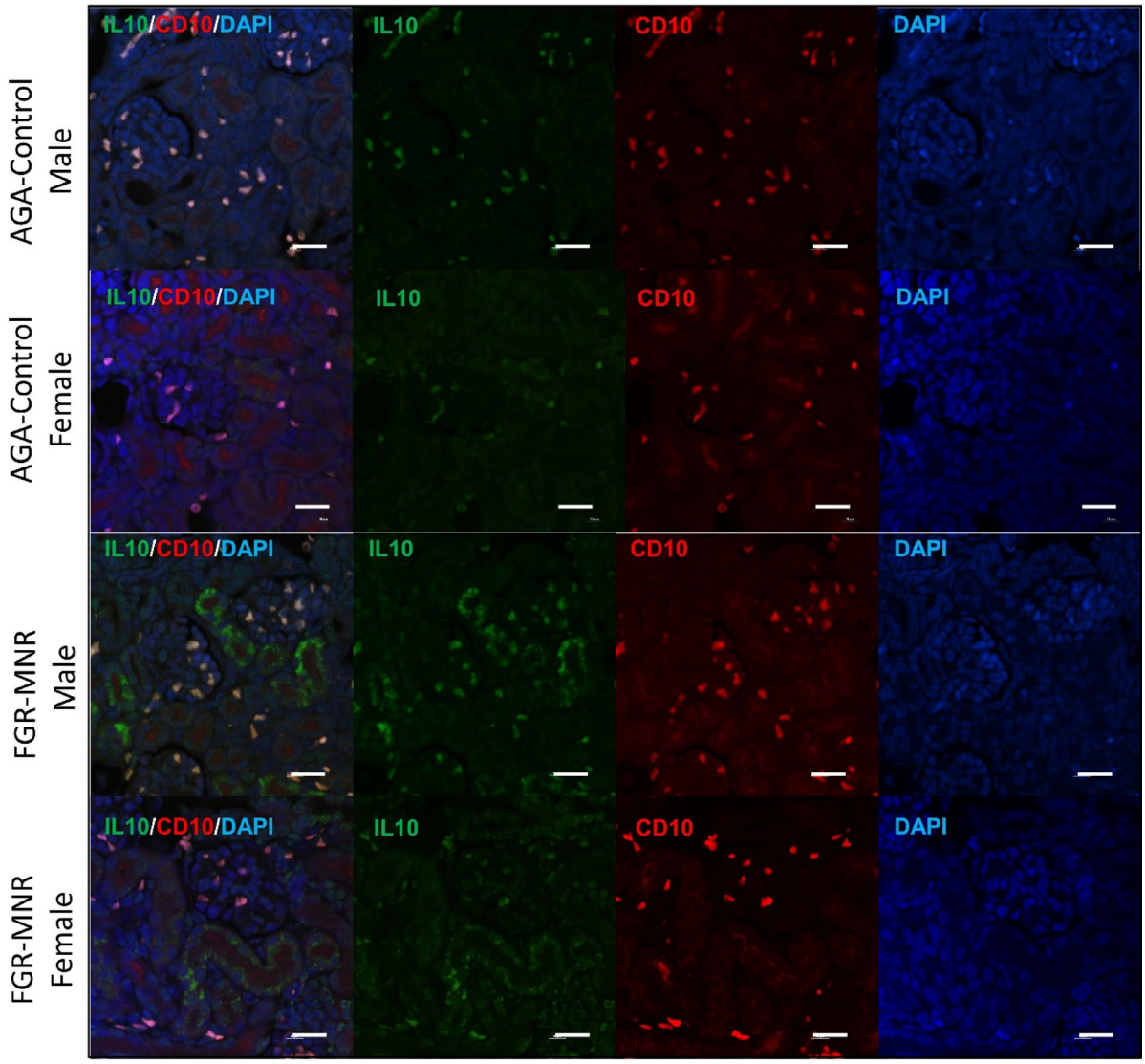


Fig. 6. Immunofluorescence localisation of IL-10 and CD10 in foetal kidneys from FGR-MNR and AGA-Control groups. Representative immunofluorescence images showing interleukin-10 (IL-10, green), CD10 (a proximal tubular marker, red), and nuclear counterstaining with DAPI (blue) in foetal kidneys from male and female guinea pigs of the AGA-Control and FGR-MNR groups. Merged images (IL-10/CD10/DAPI) demonstrate increased IL-10 expression in the renal tubules of FGR-MNR foetuses compared with AGA-Controls. Scale bars = 20 µm. AGA, appropriate-for-gestational-age; FGR-MNR, foetal growth restriction model: maternal nutrient restriction.

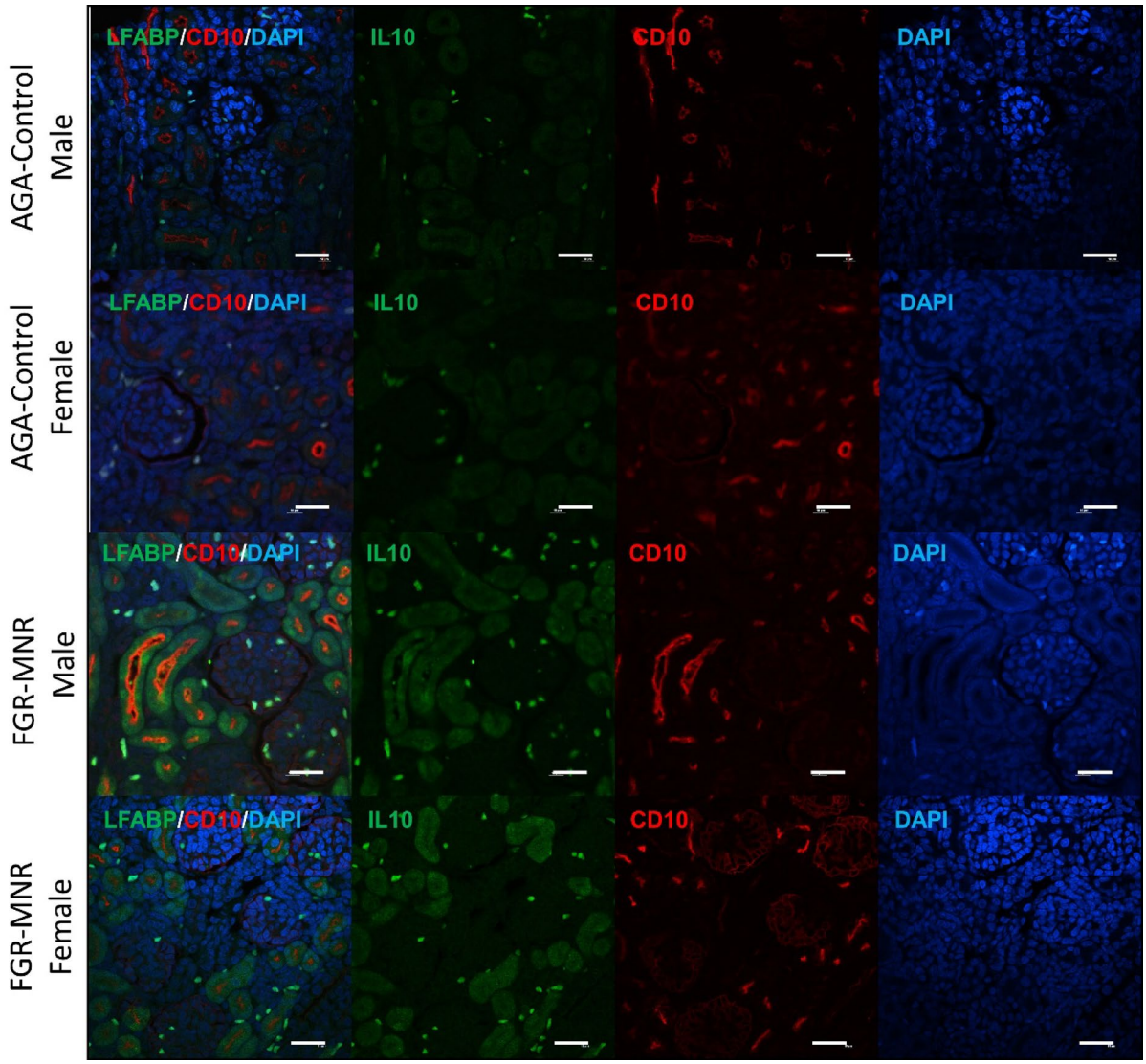


Fig. 7. Immunofluorescence localisation of L-FABP and CD10 in foetal kidneys from FGR-MNR and AGA-Control groups. Representative immunofluorescence images showing liver-type fatty acid–binding protein (L-FABP, green), CD10 (a proximal tubular marker, red), and nuclear counterstaining with DAPI (blue) in foetal kidneys from male and female guinea pigs of the AGA-Control and FGR-MNR groups. Merged images (L-FABP/CD10/DAPI) demonstrate enhanced L-FABP expression in the renal tubules of FGR-MNR foetuses compared with AGA-Controls. Scale bars = 20 μm. AGA, appropriate-for-gestational-age; FGR-MNR, foetal growth restriction model: maternal nutrient restriction.

Availability of data and materials

All original raw data used to generate graphical and tabular summary results are archived and fully available upon reasonable request.

Received: 19 November 2025; Accepted: 19 January 2026
Published online: 11 February 2026

References

1. Bernstein IM, Horbar JD, Badger GJ, Ohlsson A, Golan A. Morbidity and mortality among very-low-birth-weight neonates with intrauterine growth restriction. The Vermont Oxford Network. *Am J Obstet Gynecol.* 2000;182:198–206.
2. Resnik, R. Intrauterine growth restriction. *Obstet Gynecol.* **99**, 490–496 (2002).
3. Veille, J. C. & Kanaan, C. Duplex Doppler ultrasonographic evaluation of the fetal renal artery in normal and abnormal fetuses. *Am J Obstet Gynecol.* **161**, 1502–1507 (1989).
4. Yoshimura, S., Masuzaki, H., Gotoh, H. & Ishimaru, T. Fetal redistribution of blood flow and amniotic fluid volume in growth-retarded fetuses. *Early Hum Dev.* **47**, 297–304 (1997).
5. Lee, S. M. et al. Usefulness of fetal urine production measurement for prediction of perinatal outcomes in uteroplacental insufficiency. *J Ultrasound Med.* **33**, 2165–2171 (2014).

6. Meher, S., Hernandez-Andrade, E., Basheer, S. N. & Lees, C. Impact of cerebral redistribution on neurodevelopmental outcome in small-for-gestational-age or growth-restricted babies: a systematic review. *Ultrasound Obstet Gynecol.* **46**, 398–404 (2015).
7. Brace, R. A. Physiology of amniotic fluid volume regulation. *Clin Obstet Gynecol.* **40**, 280–289 (1997).
8. Craigo, S. D., Beach, M. L., Harvey-Wilkes, K. B. & D'Alton, M. E. Ultrasound predictors of neonatal outcome in intrauterine growth restriction. *Am J Perinatol.* **13**, 465–471 (1996).
9. Scifres, C. M., Stamilio, D., Macones, G. A. & Odibo, A. O. Predicting perinatal mortality in preterm intrauterine growth restriction. *Am J Perinatol.* **26**, 723–728 (2009).
10. Budunoglu MD, Yapca OE, Yldildiz GA, Atakan AlR. Fetal renal blood flow velocimetry and cerebro-placental ratio in patients with isolated oligohydramnios. *J Gynecol Obstet Hum Reprod.* 2019;48:495–9.
11. Elias, A. A., Ghaly, A., Matushewski, B., Regnault, T. R. & Richardson, B. S. Maternal nutrient restriction in guinea pigs as an animal model for inducing fetal growth restriction. *Reprod Sci.* **23**, 219–227 (2016).
12. Maki, Y., Nygard, K., Hammond, R. R., Regnault, T. R. & Richardson, B. S. Maternal undernourishment in guinea pigs leads to fetal growth restriction with increased hypoxic cells and oxidative stress in the brain. *Dev Neurosci.* **41**, 290–299 (2019).
13. Kind, K. L. et al. Chronic maternal feed restriction impairs growth but increases adiposity of the fetal guinea pig. *Am J Physiol Regul Integr Comp Physiol.* **288**, R119–R126 (2005).
14. Sheldon, R. E., Peeters, L. L., Jones, M. D. Jr., Makowski, E. L. & Meschia, G. Redistribution of cardiac output and oxygen delivery in the hypoxemic fetal lamb. *Am J Obstet Gynecol.* **135**, 1071–1078 (1979).
15. Wladimiroff, J. W. & van Bel, F. Fetal and neonatal cerebral blood flow. *Semin Perinatol.* **11**, 335–346 (1987).
16. Richardson, B. S. Fetal adaptive responses to asphyxia. *Clin Perinatol.* **16**, 595–611 (1989).
17. Asanuma, K. & Mundel, P. The role of podocytes in glomerular pathobiology. *Clin Exp Nephrol.* **7**, 255–259 (2003).
18. Pavenstädt, H., Kriz, W. & Kretzler, M. Cell biology of the glomerular podocyte. *Physiol Rev.* **83**, 253–307 (2003).
19. Conti, M. et al. Urinary cystatin C as a specific marker of tubular dysfunction. *Clin Chem Lab Med.* **44**, 288–291 (2006).
20. Dieterle, F. et al. Urinary clusterin, cystatin C, beta2-microglobulin and total protein as markers to detect drug-induced kidney injury. *Nat Biotechnol.* **28**, 463–469 (2010).
21. Grasselli, C. Detection of urinary cystatin-c in IUGR neonates by immunoblot SDS-PAGE. *Pediatr Neonatol.* **63**, 599–604 (2022).
22. Yamamoto T, Noiri E, Ono Y, Doi K, Negishi K, Kamijo A, et al. Renal L-type fatty acid—binding protein in acute ischemic injury. *J Am Soc Nephrol.* 2007;18:2894–2902.
23. McMahon, B. A. & Murray, P. T. Urinary liver fatty acid-binding protein: another novel biomarker of acute kidney injury. *Kidney Int.* **77**, 657–659 (2010).
24. Xu, Y., Xie, Y., Shao, X., Ni, Z. & Mou, S. L-FABP: A novel biomarker of kidney disease. *Clin Chim Acta.* **445**, 85–90 (2015).
25. Katsura, D. et al. Amniotic fluid L-type fatty acid-binding protein in predicting fetal condition. *Tohoku J Exp Med.* **254**, 267–273 (2021).
26. Katsura, D. et al. Evaluation of amniotic fluid neutrophil gelatinase-associated lipocalin and L-type fatty acid-binding protein levels during pregnancy. *Eur J Obstet Gynecol Reprod Biol X.* **21**, 100269 (2024).
27. Pachì, A. et al. Renal tubular damage in fetuses with intrauterine growth retardation. *Fetal Diagn Ther.* **8**, 109–113 (1993).
28. Kamianowska, M., Szczepański, M., Kulikowska, E. E., Bebko, B. & Wasilewska, A. The tubular damage markers: neutrophil gelatinase-associated lipocalin and kidney injury Molecule-1 in newborns with intrauterine growth restriction. *Neonatology* **115**, 169–174 (2019).
29. Takahashi, M. et al. ATP dynamics as a predictor of future podocyte structure and function after acute ischemic kidney injury in female mice. *Nat Commun.* **15**, 9977 (2023).
30. Sorrentino, G., Falzoni, P., Balossini, F. & Angeli, G. The multilocular cystic nephroma in childhood. *A case report. Minerva Pediatr.* **43**, 329–333 (1991).
31. Caruso-Neves, C., Pinheiro, A. A., Cai, H., Souza-Menezes, J. & Guggino, W. B. PKB and megalin determine the survival or death of renal proximal tubule cells. *Proc Natl Acad Sci U S A.* **103**, 18810–18815 (2006).
32. Nechemia-Arbely, Y. et al. IL-6/IL-6R axis plays a critical role in acute kidney injury. *J Am Soc Nephrol.* **19**, 1106–1115 (2008).
33. Wang, W. W. et al. IL-10 from dendritic cells but not from T regulatory cells protects against cisplatin-induced nephrotoxicity. *PLoS ONE* **15**, e0238816 (2020).
34. Yue, S. L. et al. Perinatal blood biomarkers for the identification of brain injury in very low birth weight growth-restricted infants. *J Perinatol.* **41**, 2252–2260 (2021).
35. Gamborg, M. et al. Birth weight and systolic blood pressure in adolescence and adulthood: meta-regression analysis of sex- and age-specific results from 20 Nordic studies. *Am J Epidemiol.* **166**, 634–645 (2007).
36. Sehgal, A., Alexander, B. T., Morrison, J. L. & South, A. M. Fetal growth restriction and hypertension in the offspring: mechanistic links and therapeutic directions. *J Pediatr.* **224**, 115-123.e2 (2020).
37. Gjerde, A., Lillås, B. S., Marti, H. P., Reisæter, A. V. & Vikse, B. E. Intrauterine growth restriction, preterm birth and risk of end-stage renal disease during the first 50 years of life. *Nephrol Dial Transplant.* **35**, 1157–1163 (2020).
38. Deutinger, J., Bartl, W., Pfersmann, C., Neumark, J. & Bernaschek, G. Fetal kidney volume and urine production in cases of fetal growth retardation. *J Perinat Med.* **15**, 307–315 (1987).
39. Verburg, B. O. et al. Fetal kidney volume and its association with growth and blood flow in fetal life: the Generation R Study. *Kidney Int.* **72**, 754–761 (2007).
40. Sutherland, M. R. & Black, M. J. The impact of intrauterine growth restriction and prematurity on nephron endowment. *Nat Rev Nephrol.* **19**, 218–228 (2023).

Acknowledgements

We would like to express our sincere gratitude to Mr. Takefumi Yamamoto, a technical staff member at the Central Research Laboratory, Shiga University of Medical Science, for his invaluable assistance in the preparation and imaging of electron microscopy samples. Mr Yamamoto's expertise and support were instrumental to the success of this study.

Author contributions

Ayako Inatomi contributed to the study as the principal investigator, performing data analysis, conducting animal experiments, and drafting the manuscript. Daisuke Katsura and Shinsuke Tokoro supported the conceptualisation of experimental design. Yuji Tanaka, Akiko Nakamura and Kaori Hayashi assisted with the biochemical experiments. Shunichiro Tsuji served as the supervisor of the study, overseeing its overall progress and integrity.

Funding

This work was supported by the Research Funding Grant for the Encouragement of Early Career Scientists by the SUMS President (FY2022).

Declarations

Competing interests
The authors declare no competing interests.

Ethics approval
All animal procedures were approved by the Animal Experimentation Committee of Shiga University of Medical Science (Approval No. 2023–3-9) and were performed in accordance with Japanese governmental guidelines for the care and use of laboratory animals.

Additional information
Supplementary Information The online version contains supplementary material available at https://doi.org/10.1038/s41598-026-36964-7.

Correspondence and requests for materials should be addressed to A.I.

Reprints and permissions information is available at www.nature.com/reprints.

Publisher's note Springer Nature remains neutral with regard to jurisdictional claims in published maps and institutional affiliations.

Open Access This article is licensed under a Creative Commons Attribution-NonCommercial-NoDerivatives 4.0 International License, which permits any non-commercial use, sharing, distribution and reproduction in any medium or format, as long as you give appropriate credit to the original author(s) and the source, provide a link to the Creative Commons licence, and indicate if you modified the licensed material. You do not have permission under this licence to share adapted material derived from this article or parts of it. The images or other third party material in this article are included in the article's Creative Commons licence, unless indicated otherwise in a credit line to the material. If material is not included in the article's Creative Commons licence and your intended use is not permitted by statutory regulation or exceeds the permitted use, you will need to obtain permission directly from the copyright holder. To view a copy of this licence, visit http://creativecommons.org/licenses/by-nc-nd/4.0/.

© The Author(s) 2026